A Waveform Diversity Method for Optimizing 3-D Power Depositions Generated by Ultrasound Phased Arrays

Xiaozheng (Jenny) Zeng, Jian Li, *Fellow, IEEE*, and Robert J. McGough*, *Member, IEEE*

***Abstract*—A waveform-diversity-based approach for 3-D tumor heating is compared to spot scanning for hyperthermia applications. The waveform diversity method determines the excitation signals applied to the phased array elements and produces a beam pattern that closely matches the desired power distribution. The optimization algorithm solves the covariance matrix of the excitation signals through semidefinite programming subject to a series of quadratic cost functions and constraints on the control points. A numerical example simulates a 1444-element spherical-section phased array that delivers heat to a 3-cm-diameter spherical tumor located 12 cm from the array aperture, and the results show that waveform diversity combined with mode scanning increases the heated volume within the tumor while simultaneously decreasing normal tissue heating. Whereas standard single focus and multiple focus methods are often associated with unwanted intervening tissue heating, the waveform diversity method combined with mode scanning shifts energy away from intervening tissues where hotspots otherwise accumulate to improve temperature localization in deep-seated tumors.**

***Index Terms*—Multiple focusing, thermal therapy, ultrasound phased array.**

I. Introduction

HYPERTHERMIA eliminates cancerous tissue by elevating tumor temperatures to 41 °C–43 °C [1], and focused ultrasound is an advantageous approach for delivering noninvasive treatments to deep sites. Various techniques have been developed for the effective delivery of ultrasound. For example, focal spots are scanned along spiral trajectories under MRI guidance to achieve relatively uniform temperatures [2]. Superposing beam patterns with multiple foci can require less average power and shorter times than single focus spot scanning to achieve a desired thermal dose [3], [4]. The pseudoinverse pattern synthesis method [5] is a multiple focus scanning approach that obtains a minimum-norm least-square solution to a series of linear equations, where the linear equations describe the relationship between the array excitation signals and the pressures at selected field points. Sector vortex scanning [6] and mode scanning [7] approaches generate multiple foci when rotating the phase across the array aperture to produce destructive interference along the array normal.

Waveform diversity extends multiple focus scanning [8]–[10] by generating several beam patterns to match a desired power distribution. Waveform diversity enhances the performance of multiple-input–multiple-output (MIMO) radar imaging [8] by solving a convex optimization problem that connects the power pattern to the covariance matrix of the excitation signals. Waveform diversity has also been adapted to ultrasound power optimization. Previous results were generated for a 2-D breast model with a small 1-D curvilinear array [10] that focuses energy in a single plane. Additional evaluations are needed to address intervening tissue heating and other problems that arise in large 3-D models [11]. To determine the effectiveness of waveform diversity in a 3-D model, temperatures generated by a spherical-section phased array are simulated in a deep-seated spherical tumor. Results show that spot scanning has significant problems with intervening tissue heating. In contrast, results produced by the waveform diversity method combined with mode scanning show that only moderate heating occurs in intervening tissues and that the overall normal tissue heating is reduced. Thus, waveform diversity combined with mode scanning achieves improved localization relative to spot scanning when hyperthermia is delivered to deep-seated tumors with large ultrasound phased arrays.

II. Methods

A. Waveform Diversity Calculations

For a continuous-wave excitation, the pressure generated by a phased array at a spatial coordinate $\mathbf{r}$ and at time t is defined by

$$p(\mathbf{r},t)=\sum_{m=1}^{M}p_m(\mathbf{r})w_m(t) \tag{1}$$

where M is the number of array elements, $p_m(\mathbf{r})$ is the complex pressure produced by the mth array element at $\mathbf{r}$ when excited by a sinusoidal signal with unit amplitude and zero phase, and $w_m(t)$ is a sinusoidal input multiplied by a complex weight that contains the phase and amplitude applied to the mth array element. In (1), $p(\mathbf{r},t)$ represents an individual time-harmonic beam pattern that contains multiple focal points. When an array

Manuscript received February 16, 2009; revised July 1, 2009. First published August 25, 2009; current version published January 4, 2010. This work was supported by the National Science Foundation Theoretical Foundations under Grant 0634786. *Asterisk indicates corresponding author*.

X. (Jenny) Zeng was with the Department of Electrical and Computer Engineering, Michigan State University, East Lansing, MI 48824 USA. She is now with Siemens Healthcare, Issaquah, WA 98029 USA.

J. Li is with the Department of Electrical and Computer Engineering, University of Florida, Gainesville, FL 32611 USA (e-mail: li@dsp.ufl.edu).

*R. J. McGough is with the Department of Electrical and Computer Engineering, Michigan State University, East Lansing, MI 48824 USA (e-mail: mcgough@egr.msu.edu).

Digital Object Identifier 10.1109/TBME.2009.2030787

generates a sequence of several beam patterns, (1) becomes

$$p(\mathbf{r},n)=\sum_{m=1}^{M}p_m(\mathbf{r})w_m(n)=\overline{p}(\mathbf{r})\overline{w}(n),\quad n=1,2,\ldots,N \tag{2}$$

where $\overline{p}(\mathbf{r})$ is a $1\times M$ row vector that is populated with the values $p_m(\mathbf{r})$ and $\overline{w}(n)$ is an $M\times 1$ column vector, which represents the excitation applied to the array for an individual beam pattern indexed by n. Thus, $p(\mathbf{r},n)$ describes a sequence of N different beam patterns, and the ultrasound phased array repeatedly cycles through these multiple focus patterns during the hyperthermia treatment. The power depositions from the individual beam patterns are computed with the plane-wave approximation and then superposed, giving

$$Q(\mathbf{r})=\frac{\alpha}{\rho c}\sum_{n=1}^{N}p(\mathbf{r},n)p^{*}(\mathbf{r},n) \tag{3}$$

where $Q(\mathbf{r})$ is the total power deposition, α is the absorption coefficient, ρ and c represent the density of the medium and the speed of sound, respectively, and the superscript * represents the conjugate transpose. Substituting (2) into (3), the expression for the power deposition becomes

$$Q(\mathbf{r})=\frac{\alpha}{\rho c}\sum_{n=1}^{N}\overline{p}(\mathbf{r})\overline{w}(n)\overline{w}^{*}(n)\overline{p}^{*}(\mathbf{r})=\frac{\alpha}{\rho c}\overline{p}(\mathbf{r})R\overline{p}^{*}(\mathbf{r}) \tag{4}$$

where R is an $M\times M$ Hermitian matrix that is equivalent to the covariance matrix defined in [10]. The deterministic beam synthesis problem is directly solved by sequentially assigning each column of $R^{1/2}$ to a complex array excitation $\overline{w}(n)$, where $R^{1/2}$ is the Hermitian square root of R. The matrix R is rank deficient, so the number of distinct excitation signals is significantly reduced through singular value decomposition. Here, the rank of the matrix R defines the number of discrete excitations N, and the singular value decomposition is defined as $R=USV^{*}$, where U and V are $M\times N$ matrices with orthonormal columns, and S is a diagonal $N\times N$ matrix that contains the singular values of R. The reduced solution is then represented by

$$X=US^{1/2} \tag{5}$$

where $S^{1/2}$ is the matrix square root of S, and each column of the $M\times N$ matrix X contains a distinct array excitation $\overline{w}(n)$. Thus, the number of unique array excitations required to achieve the optimal covariance matrix R is reduced from M, the number of array elements, to a much smaller number given by $N=\text{rank}(R)$.

One objective function that is commonly deployed in hyperthermia applications attempts to deliver relatively uniform power within the tumor region when minimizing the power deposition in normal tissue. The optimization problem solved here is as follows:

$$\begin{aligned}
&\min_{t,R}\ -t\\
&\text{s.t. } \overline{p}(\mathbf{r}_0)R\overline{p}^{*}(\mathbf{r}_0)-\overline{p}(\mu)R\overline{p}^{*}(\mu)>t, && \mu\in\Omega_N\\
&\quad \overline{p}(\nu)R\overline{p}^{*}(\nu)\geq 0.9\overline{p}(\mathbf{r}_0)R\overline{p}^{*}(\mathbf{r}_0), && \nu\in\Omega_T\\
&\quad \overline{p}(\nu)R\overline{p}^{*}(\nu)\leq 1.1\overline{p}(\mathbf{r}_0)R\overline{p}^{*}(\mathbf{r}_0), && \nu\in\Omega_T\\
&\quad R\geq 0\\
&\quad \sum R_{mm}=\gamma
\end{aligned} \tag{6}$$

where μ denotes one of the N_N control points in the normal tissue region Ω_N, ν denotes one of the N_T control points in the tumor region Ω_T, and $\mathbf{r}_0$ is a characteristic point within Ω_T, i.e., $\mathbf{r}_0$ is a representative point in the tumor. The cost function maximizes the difference between the power at r_0 and the power at all normal tissue control points μ, given that this difference is nonnegative. The first constraint (combined with the restriction $t>0$) guarantees that the power at $\mathbf{r}_0$ is always larger than the power at μ. The second and the third constraints ensure that the power deposited at the tumor control points ν is not more than 1.1 times and not less than 0.9 times the power at $\mathbf{r}_0$. The fourth constraint defines the matrix R as a positive semidefinite Hermitian matrix. The fifth constraint indicates that the total input power is specified by the constant γ [8]. The first four constraints are the same as in [10], and the fifth constraint in (6) specifies the total input power instead of an average uniform power. The function $p(\mathbf{r})=\overline{p}(\mathbf{r})R\overline{p}^{*}(\mathbf{r})$ is convex; therefore, the optimization problem in (6) can be solved with public domain software for convex optimization, e.g., SeDuMi [12] or SDPT3 [13].

B. Spot Scanning

An ultrasound phased array generates a focus by adjusting the phases of the excitation signals. For continuous-wave excitations, a single focus is produced by phase conjugation [14], where the negative of the phase of the complex pressure transfer function evaluated at the focus for each array element defines the phase of the excitation signal for that element. With this approach, the phased array generates constructive interference at each focal spot.

C. Mode Scanning

Symmetric multiple focusing is realized with mode scanning [7]. Mode scanning utilizes the symmetry of the phased array to generate a symmetric focal pattern while canceling the pressure along one or more planes of symmetry. A symmetric phased array is typically divided by these symmetric planes into two or four equal sections. The array elements in each section are indexed according to the planes of symmetry such that the distances from each pair of elements to any point on the plane of symmetry are equal. The computational volume is also divided into an equal number of sections by these same planes of symmetry. The rotational signals are defined such that the phases applied to elements on opposite sides of each plane of symmetry are offset by π, which causes pressure cancelations along the planes of symmetry. A symmetric, focused power distribution is formed by applying rotational excitation signals to each

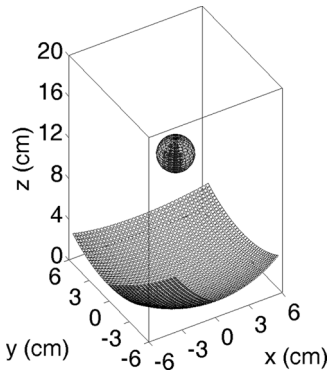

Fig. 1. Spherical section array with 1444 square elements heats a 3-cm spherical tumor model located 12 cm from the bottom of the array. One quarter of the array (361 elements) is highlighted and the corresponding focal points in one quadrant (34 of 136 total focal points) are illustrated to emphasize the symmetry of each component in simulations that combine waveform diversity with mode scanning.

symmetric group of elements and then calculating the phase of each group with phase conjugation or waveform diversity.

D. Pressure and Temperature Simulations

The pressures $p_m(\mathbf{r})$ generated by the individual array elements at individual control points are computed with the fast near-field method [15]. The pressure field in a 3-D volume for an array excitation $\overline{w}(n)$ is calculated with the angular spectrum approach combined with the fast near-field method [16]. The fast near-field method calculates the pressure generated by the phased array in an input plane, and the angular spectrum approach propagates the pressure in the 3-D volume. Each steady-state power deposition is computed according to (3), and the contributions from N scans are then superposed.

The temperature is simulated with the steady-state bioheat transfer equation

$$K\nabla^2 T(\mathbf{r}) - W_b C_b T(\mathbf{r}) + Q(\mathbf{r}) = 0 \tag{7}$$

where K is the thermal conductivity of tissue, C_b is the specific heat of blood, W_b is the blood perfusion rate, and T is the tissue temperature increase relative to the baseline arterial blood temperature (37 °C). Equation (7) is solved with an iterative finite-difference scheme [17].

III. Numerical Results

A. Phased Array Geometry and Spherical Tumor Model

A large spherical section array and a spherical tumor model are depicted in Fig. 1. The array consists of 1444 square elements, where each element is 0.24 cm $\times$ 0.24 cm. The bottom of the array is located at the origin of the coordinate system. The array is geometrically focused at 12 cm, and the opening angles in the lateral dimensions are 60°. The diameter of the spherical tumor is 3 cm, and the center of the tumor is located at (0, 0, 12) cm. The computational grid is defined as a 15 cm $\times$ 15 cm $\times$ 15.9 cm volume that extends from -7.5 to 7.5 cm in the x- and y-directions and from 4.05 to 19.95 cm in the z-direction. In all simulations, the following acoustic and thermal parameters are used: $\rho = 1000$ kg/m^3, $c = 1500$ m/s, $\alpha = 0.5$ dB/cm/MHz, $W_b = 5$ kg/m^3/s, $K = 0.55$ W/m/°C, and $C_b = 4000$ J/kg/°C. The excitation signal for the array has a center frequency of 1 MHz, which corresponds to a wavelength of $\lambda = 1.5$ mm.

The numerical simulations are performed on a 64-bit computer with a 2.4-GHz dual-core processor and 4 GB of RAM. The optimization routines are implemented in MATLAB. The pressure and temperature simulation routines are written in C and called as C-MEX functions by MATLAB.

B. Spot Scanning Simulations

For single focus spot scanning, 136 focal points are distributed within the spherical tumor. The focal spots are organized in concentric rings with 0.45 cm (3λ) spacing in the z-direction. The total power deposition is the superposition of power depositions produced by all 136 points. The steady-state temperature field is then calculated with the bioheat transfer equation using the total power deposition calculated with spot scanning. In these simulations, the power distribution is scaled such that the overall peak temperature increase is 6 °C.

The resulting temperature rise in the xy-plane across the center of the tumor is shown in Fig. 2(a), and the temperature rise in the yz-plane at $x = 0$ is shown in Fig. 2(b). Fig. 2 shows the 1 °C, 2 °C, 3 °C, 4 °C, and 5 °C isothermal contours, where the 4 °C and 5 °C contours are drawn with thicker lines to indicate the regions that achieve temperatures appropriate for hyperthermia and heat-modulated drug delivery [18]. The circle (dashed line) in Fig. 2 illustrates the diameter of the spherical tumor. In Fig. 2(a), the 2 °C contour is almost coincident with the tumor boundary, and the 4 °C and 5 °C contours are concentric rings that are located inside of the tumor boundary. Fig. 2(b) indicates that the peak temperature occurs in the proximal tumor region and that a significant portion of the periphery is underheated. Fig. 3 shows the spatial relationship between the corresponding 4 °C isothermal surface and the 3-cm-diameter spherical tumor volume. Fig. 3 also demonstrates that spot scanning produces significant intervening tissue heating between the proximal tumor boundary and the phased array. Quantitative evaluation of the results obtained with spot scanning shows that 40.9% of the tumor volume achieves a temperature rise of 4 °C or more and 4.9 cm^3 of the normal tissue volume exceeds 4 °C.

C. Waveform Diversity Simulations

A sequence of beam patterns is also synthesized with the waveform diversity method. To reduce the computational cost due to the large number of transducer elements in the array, the spherical section array is divided into four quadrants, and mode scanning [7] is combined with waveform diversity optimization. The control points are accordingly divided into four groups. The array elements are excited with rotational phases in groups of four as specified by the mode scanning technique, and this combination of elements is then optimized with the waveform diversity method. Consequently, a sequence of symmetric focal patterns with multiple foci are formed in the tumor. The symmetric array and focal point geometries are illustrated

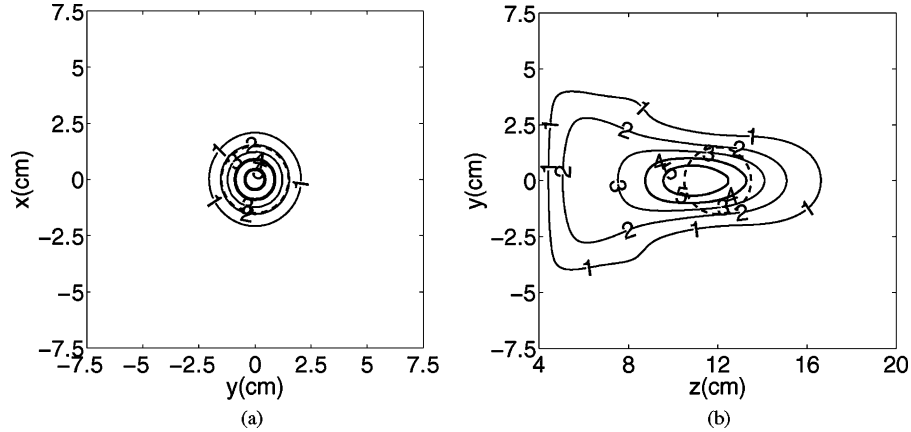

Fig. 2. Simulated temperature rise (in degrees Celsius) generated by single focus spot scanning in a 3-cm-diameter spherical tumor. Cross sections are shown in the xy-plane at $z = 12$ cm in Fig. 2(a) and in the yz-plane at $x = 0$ in Fig. 2(b). The overall peak temperature is $6\,^{\circ}$C. (a) Temperature rise in the xy-plane at $z = 12$ cm. (b) Temperature rise in the yz-plane at $x = 0$.

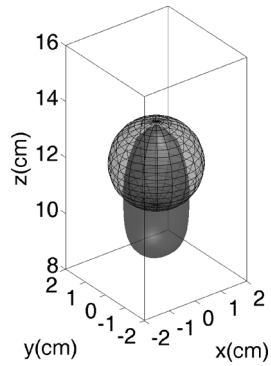

Fig. 3. 3 cm spherical tumor model and the $4\,^{\circ}$C isothermal surface generated by single focus spot scanning.

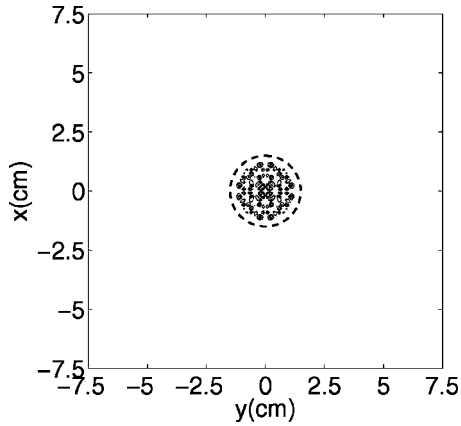

Fig. 4. Simulated power deposition obtained from the superposition of $N = 3$ multiple focus scans generated by waveform diversity optimization combined with mode scanning. This cross section is shown in the xy-plane at $z = 12$ cm.

in Fig. 1, where the 361 array elements in quadrant III (with negative x- and y-coordinates) are indicated by the solid dark squares and the tumor control points in quadrant III are indicated by dots.

The locations of the focal spots are the same as those defined for spot scanning, but only one quarter of the focal points is utilized in waveform diversity simulations. Of the 34 focal points in quadrant III, 33 of these are identified as tumor control points ν, and one arbitrarily selected point is the reference point r_0. Within quadrant III, 144 normal tissue control points μ are uniformly distributed within a square 0.825 cm $\times 0.825$ cm grid located in the xy-plane at $z = 9.45$ cm with 0.075 mm $(\lambda/2)$ spacing in each direction. This distribution of normal tissue control points reduces intervening tissue heating when shifting the peak temperatures toward the center of the tumor model.

After the optimized covariance matrix R is obtained from SeDuMi or SDPT3, the eigenvalues of the covariance matrix are computed with MATLAB. The rank, which is defined here as the number of eigenvalues that are greater than or equal to 1% of the largest eigenvalue, is then computed. For this combination of array geometry, tissue parameters, and control points, $\text{rank}(R) = 3$. Thus, to obtain the results of the waveform diversity simulations, only $N = 3$ different array excitations are required to generate 34 foci in quadrant III and 136 foci overall when simultaneously minimizing the power delivered to the 144 normal tissue control points in quadrant III and 576 normal tissue control points overall. The complex array excitations $\overline{w}(n)$ are subsequently synthesized from R according to (5). The pressures generated by the phased array are then computed for these excitation signals, and the power depositions for $N = 3$ multiple focus scans are superposed. The total power deposition in Fig. 4 depicts contours evaluated at 20% intervals in the xy-plane at $z = 12$ cm. Fig. 4 indicates that the power peaks in this cross section are confined within the tumor diameter indicated by the dashed line.

The temperature distributions in the xy-plane at $z = 12$ cm and in the yz-plane at $x = 0$ are shown in Fig. 5(a) and (b), respectively. Fig. 5(b) shows that, with waveform diversity, the peak temperatures are located near the center of the tumor, and the centers of the $4\,^{\circ}$C and $5\,^{\circ}$C isothermal contours are almost coincident with the center of the spherical tumor. A 3-D isothermal contour indicating the corresponding volume that achieves a $4\,^{\circ}$C temperature rise is shown in Fig. 6. Figs. 5 and 6 demonstrate that waveform diversity combined with mode scanning eliminates a significant amount of the intervening tissue heating. Quantitative evaluation of the waveform diversity results indicate that 56.5% of the tumor volume achieves a temperature

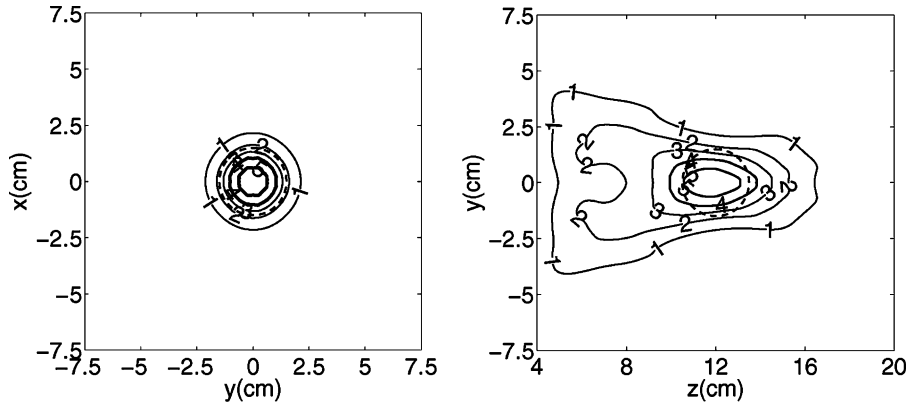

(a) (b)

Fig. 5. Simulated temperature rise (in degrees Celsius) generated by waveform diversity combined with mode scanning in a 3-cm-diameter spherical tumor. Cross sections are shown in the xy-plane at $z = 12$ cm in Fig. 5(a) and in the yz-plane at $x = 0$ in Fig. 5(b). The overall peak temperature is $6\,^{\circ}$C. (a) Temperature rise in the xy-plane at $z = 12$ cm. (b) Temperature rise in the yz-plane at $x = 0$.

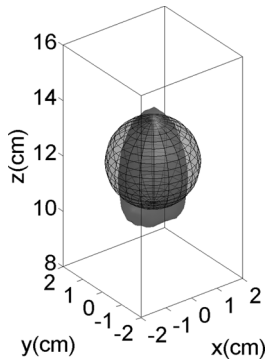

Fig. 6. 3-cm spherical tumor model and the $4\,^{\circ}$C isothermal surface generated by waveform diversity combined with mode scanning.

rise of $4\,^{\circ}$C or more, and 2.0 cm^3 of the normal tissue volume exceeds $4\,^{\circ}$C. With this combination of tumor and normal tissue control points, waveform diversity combined with mode scanning increases the heated tumor volume by 38% while decreasing the heated normal tissue volume by 59% relative to single spot scanning.

IV. Discussion

A. Control Point Distribution

The distribution of control points strongly influences the results obtained with the waveform diversity method. In initial parametric evaluations of the waveform diversity method, tumor control points were distributed uniformly within the 3-cm-diameter sphere with different spacings between adjacent points. The results indicate that a more densely populated tumor control point distribution improves the tumor coverage when increasing normal tissue temperatures. The tumor control point distribution evaluated here was in part selected as a compromise between the conflicting tumor and normal tissue temperature objectives and was in part determined by the amount of computer RAM available for the initial computer simulations.

In an effort to determine an effective distribution that reduces normal tissue heating, distributions of normal tissue control points were evaluated in several different locations, including between the array and the proximal edge of the tumor, beyond the distal edge of the tumor, and different combinations of these two locations. Tissue control points located beyond the tumor were largely ineffective, which suggests that the axial heating beyond the distal edge of the tumor is an unavoidable consequence of the selected tumor control point distribution. Tissue control points located between the array and the proximal tumor edge tend to shift energy away from the z-axis, where peak temperatures occur despite the axial pressure field cancelations produced by mode scanning. When tissue control points were placed between the array and the tumor, the normal tissue heating was consistently reduced in this region. Of the normal tissue control point distributions evaluated, the results in Figs. 4–6 demonstrated the smallest volume of normal tissue heated above $4\,^{\circ}$C and one of the smallest $4\,^{\circ}$C tumor coverages associated with this tumor control point distribution. Waveform diversity combined with mode scanning readily achieves $4\,^{\circ}$C tumor coverage in excess of 60% with $4\,^{\circ}$C normal tissue volumes that are well below 3 cm^3 when other normal tissue control point distributions are applied to this combination of array and tumor parameters.

Additional evaluations of distribution strategies for tumor and normal tissue control points are still needed. Both spot scanning and waveform diversity consistently underheat the tumor periphery, particularly in locations far from the z-axis. Modified control point placement strategies are expected to achieve further improvements in the waveform diversity results. One possible strategy places a higher density of tumor control points near the tumor edge, and another includes tumor control points outside of the tumor volume. Other strategies potentially consider different constraints and/or objective functions to improve conformal tumor heating. These and other extensions of the waveform diversity method will be evaluated in future research.

B. Uniform Array Excitation

An alternative constraint specifies equal values for the diagonal entries in the covariance matrix R [10]. The excitations satisfying this constraint achieve uniform power across the array

aperture in the sense that when the squares of the absolute values of the entries in the excitation matrix X are added across each row, the result is a column vector with equal entries. However, when the absolute value of the excitation applied to each array element is evaluated and the columns of X are considered individually, the individual excitations are highly nonuniform. Thus, the main advantages of uniform excitations for hyperthermia are not achieved with this particular constraint. Furthermore, when the optimization procedure attempts to achieve an array excitation that is uniform or nearly uniform, contributions from eigenvectors that oppose the tumor and normal tissue objectives are necessarily included in the uniform excitation solution. These issues motivate the expression in (6), which achieves more conformal tumor heating and lower normal tissue temperatures than the uniform excitation solution in [10].

C. Computational Cost

One limitation of the waveform diversity method is the high computational cost. An ultrasound phased array applicator designed for deep hyperthermia usually requires hundreds or thousands of array elements, and the computer memory required for waveform diversity optimization is approximately proportional to the square of the number of array elements. Increasing the number of control points also adds to the computational burden. According to (6), the number of constraint functions is equal to $N_N + 2N_T + 1$, and the number of unknowns is $N_N + 2N_T + M^2 + 1$, where M is the number of transducer elements, and N_N and N_T represent the number of control points in normal tissue and the tumor, respectively. An intermediate sparse $(N_N + 2N_T + 1) \times (N_N + 2N_T + M^2 + 1)$ matrix is constructed during the optimization process, where the number of nonzero entries in the matrix is $N_N(2 + M^2) + 2N_T(1 + M^2) + M$. The huge amount of data prevents the waveform diversity method from directly optimizing large arrays on many desktop computer systems. For example, waveform diversity calculations with the full 1444 element array using 135 tumor control points, and 576 tissue control points require approximately 40 GB just to store this intermediate matrix. However, if mode scanning is used in conjunction with waveform diversity, the computational cost is reduced considerably. When the spherical section array and the control points are divided into four quadrants according to the symmetry of the array and the spherical tumor model, a total of 361 array elements, 33 tumor control points and 144 tissue control points are used, and the computer memory required for this intermediate matrix is reduced to 626 MB. The time required to optimize the solution for waveform diversity solution combined with mode scanning is about half an hour on a computer with a 64-bit operating system and 4 GB of RAM. Solving the full aperture problem on a 64-bit computer with additional RAM requires much more time.

D. Advantages Over Traditional Multiple Focus Beamforming

The waveform diversity method has several advantages over traditional multiple focusing approaches. First, waveform diversity combined with mode scanning determines an optimal combination of several multiple focus patterns, whereas traditional multiple focusing typically attempts to optimize individual multiple focus patterns separately without considering the interactions between the beam patterns. Second, waveform diversity combined with mode scanning facilitates optimal energy deposition at hundreds of tumor and normal tissue control points with a small number (in the example shown here, $N = 3$) of multiple focus patterns. Traditional multiple focusing approaches are also capable of controlling the field at a large number of points; however, the traditional approaches tend to generate unintended hotspots as the number of focal points becomes large. Third, simulations of waveform diversity have demonstrated simultaneous control over the power deposition in the tumor and in normal tissues, whereas traditional multiple focusing tends to concentrate primarily on power delivery in the tumor. Preliminary evaluations indicate that waveform diversity achieves these two objectives simultaneously at a large number of locations without causing excessive hot spots in undesirable locations. Fourth, waveform diversity is very flexible in that several different types of constraints are available. Inequality or equality constraints can be applied to the array excitation, the tumor control points, and the normal tissue control points, and each combination produces a different covariance matrix R that ultimately determines the power deposition and the temperature distribution for hyperthermia.

V. Conclusion

Single focus spot scanning and waveform diversity combined with mode scanning are evaluated for hyperthermia with a 1444-element spherical section array that focuses ultrasound within a 3-cm-diameter tumor target located 12 cm from the array. The simulation results show that the peak tumor temperatures produced by spot scanning occur in the region of the tumor that is proximal to the phased array, and significant intervening tissue heating is also generated. For the same distribution of focal points within the tumor volume, the peak temperatures produced by waveform diversity combined with mode scanning are closer to the center of the tumor, and the intervening tissue heating is reduced significantly. For the combination of simulation parameters evaluated here, waveform diversity combined with mode scanning increases the heated volume within the tumor by 38% and simultaneously decreases normal tissue heating by 59%, where the extent of the heated volume is defined by the $4\,^{\circ}\mathrm{C}$ isothermal contour. Thus, waveform diversity combined with mode scanning generates multiple focus patterns that maximize the power delivered to the tumor when minimizing the power in other specified locations, and this combination improves the temperature localization relative to single focus spot scanning.

Acknowledgment

The authors would also like to thank B. Guo and X. Zhu for their constructive comments.

References

[1] P. R. Stauffer, "Evolving technology for thermal therapy of cancer," *Int. J. Hyperthermia*, vol. 21, no. 8, pp. 731–744, 2005.

[2] R. Salomir, J. Palussiere, F. C. Vimeux, J. A. de Zwart, B. Quesson, M. Gauchet, P. Lelong, J. Pergrale, N. Grenier, and C. T. W. Moonen,

"Local hyperthermia with MR-guided focused ultrasound: Spiral trajectory of the focal point optimized for temperature uniformity in the target region," *J. Magn. Reson. Imaging*, vol. 12, no. 4, pp. 571–583, 2000.

[3] D. R. Daum and K. Hynynen, "Thermal dose optimization via temporal switching in ultrasound surgery," *IEEE Trans. Ultrason., Ferroelectr., Freq. Control*, vol. 45, no. 1, pp. 208–215, Jan. 1998.

[4] H. Wan, J. Aarsvold, M. O'Donnell, and C. Cain, "Thermal dose optimization for ultrasound tissue ablation," *Int. J. Hyperthermia*, vol. 46, no. 4, pp. 913–928, 1999.

[5] E. S. Ebbini and C. A. Cain, "Multiple-focus ultrasound phased-array pattern synthesis: Optimal driving signal distributions for hyperthermia," *IEEE Trans. Ultrason., Ferroelectr. Freq. Control*, vol. 36, no. 5, pp. 540–548, Sep. 1989.

[6] C. A. Cain and S.-i. Umemura, "Concentric-ring and sector-vortex phased-array applicators for ultrasound hyperthermia," *IEEE Trans. Microw. Theory Tech.*, vol. MTT-34, no. 5, pp. 542–551, May 1986.

[7] R. J. McGough, H. Wang, E. S. Ebbini, and C. A. Cain, "Mode scanning: Heating pattern synthesis with ultrasound phased arrays," *Int. J. Hyperthermia*, vol. 10, no. 3, pp. 433–442, 1994.

[8] P. Stoica, J. Li, X. Zhu, and B. Guo, "Waveform synthesis for diversity-based transmit beampattern design," *IEEE Trans. Signal Process.*, vol. 56, no. 6, pp. 2593–2598, Jun. 2008.

[9] B. Guo, L. Xu, and J. Li, "Time reversal based microwave hyperthermia treatment of breast cancer," *Microw. Opt. Technol. Lett.*, vol. 47, no. 4, pp. 335–338, 2005.

[10] B. Guo and J. Li, "Waveform diversity based ultrasound system for hyperthermia treatment of breast cancer," *IEEE Trans. Biomed. Eng.*, vol. 55, no. 2, pp. 822–826, Feb. 2008.

[11] E. G. Moros, R. B. Roemer, and K. Hynynen, "Pre-focal plane high-temperature regions induced by scanning focused ultrasound beams," *Int. J. Hyperthermia*, vol. 6, no. 2, pp. 351–366, 1990.

[12] J. F. Sturm, "Using SeDuMi 1.02, a MATLAB toolbox for optimization over symmetric cones," *Optim. Methods Softw.*, vol. 11/12, pp. 625–653, 1999.

[13] K. C. Toh, M. J. Todd, and R. H. Tutuncu, "SDPT3—A MATLAB software package for semidefinite programming," *Optim. Methods Softw.*, vol. 11, pp. 545–581, 1999.

[14] M. S. Ibbini and C. A. Cain, "A field conjugation method for direct synthesis of hyperthermia phased-array heating patterns," *IEEE Trans. Ultrason., Ferroelectr. Freq. Control*, vol. 36, no. 2, pp. 3–9, Nov. 1989.

[15] R. J. McGough, "Rapid calculations of time-harmonic nearfield pressures produced by rectangular piston," *J. Acoust. Soc. Amer.*, vol. 115, no. 5, pp. 1934–1941, 2004.

[16] X. Zeng and R. J. McGough, "Optimal simulations of ultrasonic fields produced by large thermal therapy arrays using the angular spectrum approach," *J. Acoust. Soc. Amer.*, vol. 125, no. 5, pp. 2967–2977, 2009.

[17] K. B. Ocheltree and L. A. Frizzell, "Determination of power deposition patterns for localized hyperthermia: A steady state analysis," *Int. J. Hyperthermia*, vol. 3, no. 3, pp. 269–279, 1987.

[18] G. Kong and M. W. Dewhirst, "Hyperthermia and liposomes," *Int. J. Hyperthermia*, vol. 15, no. 5, pp. 345–370, 1999.